Economic Scheduling of Gaseous-liquid Hydrogen Generation and Storage Plants Considering Complementarity of Multiple Products

Jiamei Zhang, Kai Sun, *Senior Member*, *IEEE*, Canbing Li, *Senior Member*, *IEEE*, Hui Liu, *Senior Member*, *IEEE*, Wentao Huang, *Senior Member*, *IEEE*, Bin Zhou, *Senior Member*, *IEEE*, and Xiaochao Hou

***Abstract*—The accessible and convenient hydrogen supply is the foundation of successful materialization for hydrogen-powered vehicles (HVs). This paper proposes a novel optimal scheduling model for gaseous-liquid hydrogen generation and storage plants powered by renewable energy to enhance the economic feasibility of investment. The gaseous-liquid hydrogen generation and storage plant can be regarded as an energy hub to supply concurrent service to both the transportation sector and ancillary market. In the proposed model, the power to multi-state hydrogen (P2MH) process is analyzed in detail to model the branched hydrogen flow constraints and the corresponding energy conversion relationship during hydrogen generation, processing, and storage. To model the coupling and interaction of diverse modules in the system, the multi-energy coupling matrix is developed, which can exhibit the mapping of power from the input to the output. Based on this, a multi-product optimal scheduling (MPOS) algorithm considering complementarity of different hydrogen products is further formulated to optimize dispatch factors of the energy hub system to maximize the profit within limited resources. The demand response signals are incorporated in the algorithm to further enhance the operation revenue and the scenario-based method is deployed to consider the uncertainty. The proposed methodology has been fully tested and the results demonstrate that the proposed MPOS can lead to a higher rate of return for the gaseous-liquid hydrogen generation and storage plant.**

***Index Terms*—Demand response, energy hub, hydrogen generation and storage plant, optimal scheduling, renewable energy.**

Manuscript received: April 25, 2021; revised: July 27, 2021; accepted: December 21, 2021. Date of CrossCheck: December 21, 2021. Date of online publication: January 24, 2022.

This work was supported by the National Natural Science Foundation of China (No. 51877117) and the Key Project of National Natural Science Foundation of China (No. 61733010).

J. Zhang and B. Zhou are with the College of Electrical and Information Engineering, Hunan University, Changsha 410082, China, and they are also with the Hunan Key Laboratory of Intelligent Information Analysis Integrated Optimization for Energy Internet, Hunan University, Changsha 410082, China (e-mail: zhangjiamei@hnu.edu.cn; binzhou@hnu.edu.cn).

K. Sun (corresponding author) and X. Hou are with the Department of Electrical Engineering, Tsinghua University, Beijing 100084, China (e-mail: sunkai@mail.tsinghua.edu.cn; houxiaochao@tsinghua.edu.cn).

C. Li and W. Huang are with the Department of Electrical Engineering, Shanghai Jiao Tong University, Shanghai 200240, China (e-mail: licanbing@sjtu.edu.cn; hwt8989@sjtu.edu.cn).

H. Liu is with College of electrical Engineering, Guangxi University, Nanning 530004, China (e-mail: hughlh@126.com).

DOI: 10.35833/MPCE.2021.000260

NOMENCLATURE

A. Indices and Sets

ΔT	Time slot for an hour
d	Time slot for a day
NT	Study period
s, NS	Index and number of sampling scenarios
t, k	Time indexes

B. Parameters

Π^{P2H}	Conversion coefficient of power to electrolyzer
Π^{com}, Π^{ref}	Energy consumption coefficients for compressor and refrigerator
η^{pv}, η^{wt}, η^{elz}, η^{com}, η^{ref}	Efficiencies of photovoltaic unit, wind turbine, electrolyzer, compressor, and refrigerator
$\gamma^{l,d}$	Daily evaporation rate of liquid hydrogen
ρ	Probability of scenarios
C^{g}, C^{l}	Investment costs of gaseous tank and liquid reservoir
C^{EP}	Electric energy consumption cost
C^{TP}	Total hydrogen transport cost
C^{pv}, C^{wt}	Feed-in prices for photovoltaic units and wind turbines
C^{e}	Electricity price
C^{elz}, C^{com}, C^{ref}	Investment costs of electrolyzer, compressor, and refrigerator
DR^{prc}	Demand response price
GH^{prc}, LH^{prc}	Selling prices of gaseous and liquid hydrogen
k_c	Polytropic exponent of compression
$OPEX$	Operation expenditure of hydrogen generation, processing, and storage devices
OC^{elz}, OC^{com}, OC^{ref}	Operation expenditures of electrolyzer, compressor, and refrigerator

OC^g, OC^l Operation expenditures of gaseous tank and liquid reservoir

p^{stg}, p^{elz} Pressures of hydrogen storage tank and electrolyzer

$P^{pv,\max}$, $P^{wt,\max}$ Maximum output power of photovoltaic units and wind turbines

P^{DR} Demand response signal

Q^g, Q^l Accumulated gaseous hydrogen in tank and liquid hydrogen in reservoir

$Q^{g,\text{int}}$, $Q^{l,\text{int}}$ Initial hydrogen quantities of gas tank and liquid reservoir

$Q^{g,\max}$, $Q^{g,\min}$ The maximum and minimum capacities of gas tank

$Q^{l,\max}$, $Q^{l,\min}$ The maximum and minimum capacities of liquid reservoir

r^b Uncondensed hydrogen gas quality in refrigerator

r^m Mainstream of hydrogen gas in refrigerator

r^{hd} Hydrogen demand

$r^{elz,\max}$, $r^{elz,\min}$ Upper and lower limits of operation power for electrolyzer

$r^{com,\max}$, $r^{com,\min}$ Upper and lower limits of operation power for compressor

$r^{ref,\max}$, $r^{ref,\min}$ Upper and lower limits of operation power for refrigerator

R Gas constant

R^{TE} Revenue from hydrogen product selling and ancillary service provision

R^H Revenue from hydrogen product selling

R^{DR} Revenue from demand response

SOC^g, SOC^l State of charge (SOC) for gas tank and SOC for liquid reservoir

$SOC^{g,\max}$, $SOC^{g,\min}$ Upper and lower limits of SOC for gas tank

$SOC^{l,\max}$, $SOC^{l,\min}$ Upper and lower limits of SOC for liquid reservoir

TC^g, TC^l Transport costs of gaseous and liquid hydrogen

T^{P2H} Temperature of power to hydrogen

v^g, v^l Dispatch factors of input energy to produce gaseous and liquid hydrogen

y Liquefaction rate

z Ratio of gas diverted through expander

C. Variables

$f_{elz}(r^l)$ Hydrogen feeding rate from electrolyzer to refrigerator

L^e Electrical load

P^{elz} Electrolyzer power

P^{com}, P^{liq} Hydrogen compression and liquefaction power

P^{DRM} Slack variable of demand response

P^{pv}, P^{wt} Output power of photovoltaic units and wind turbines

P^g Power fed by the grid

r^{gd}, r^{ld} Gaseous and liquid hydrogen selling rates

r^{gs}, r^{ls} Hydrogen storage rates of gaseous and liquid hydrogen tanks, which are positive when the hydrogen is discharged, otherwise negative

r^{elz} Hydrogen generation rate of electrolyzer

r^g, r^l Gaseous and liquid hydrogen generation rates

I. Introduction

CARBON emissions of the transportation sector account for a large percent of the total carbon emissions. Hydrogen technologies are the promising ones to realize carbon neutralization, which can effectively reduce carbon emission [1]-[4] and promote renewable energy accommodation [5]-[7]. A crucial step towards the application of hydrogen transportation is to achieve a cost-efficient hydrogen supply [3].

For mobile applications, as much hydrogen as possible should be carried onboard to achieve a long-running distance. High-pressure gaseous hydrogen, generally 700 bar, and cryogenic liquid hydrogen, below 21 K, are the two most common hydrogen storage forms [8]-[12]. The other emerging hydrogen storage solutions can be divided into two categories, i. e., chemisorption and physisorption [3], [10], [13]. The former contains chemical hydrides, metal hydrides, and liquid organic hydrogen carriers (LOHCs). The latter includes carbon nanotubes and metal-organic frameworks (MOFs). However, these hydrogen carrier substances are initially investigated for onboard hydrogen storage [3]. Consequently, besides the development of new hydrogen storage techniques, the reasonable generation, storage, and transportation of gaseous and liquid hydrogen are crucial for the expansion of hydrogen-based transportation. The hydrogen compression is not energy-intensive, but the high-pressure storage tank is cost-intensive (600 $/kg) due to strict material requirements. It is to be regretted that the energy density of compressed hydrogen is still low [8]-[10]. Regarding liquid hydrogen, it can be stored in a cryogenic insulation reservoir at low pressure (<10 bar) with high energy densities, and its investment costs (30 $/kg) are lower than gaseous hydrogen [9]-[14]. But the liquefaction of hydrogen is energy-intensive, accounting for nearly one-third of hydrogen energy contents [13]-[15]. Besides, lower transportation costs can be achieved with higher energy density owing to the limited volume and weight of the trailer [3]. Therefore, liquid hydrogen is more suitable for large-scale long-distance transportation [11].

It should be noted that either the compressed gaseous hydrogen or the cryogenic liquid hydrogen has advantages and limitations, which can be deployed comprehensively to enhance the economic feasibility of investment. Therefore, the development of a new model to optimize the scheduling of multi-state hydrogen generation and storage is necessary.

As the sharp proliferation of renewable energy, hydrogen generation and storage powered by renewable energies, at-

tracts more attention recently [16]-[18]. A hierarchical energy management scheme was developed to improve the profit of an island hydrogen-based microgrid in [17]. Considering the complementarity of multiple energies, an optimal scheduling model was formulated in [18] for an electricity-gas-hydrogen microgrid to enhance energy utilization efficiency. It is worth noting that the hydrogen storage-based microgrids possess stacked advantages, e. g., renewable energy accommodation, demand-supply balance, and voltage stability. The investigation results of [19] showed that incentivizing wind power with hydrogen generation and storage was more cost-efficient. A novel seasonal hydrogen storage strategy was proposed in [6] to decrease renewable energy spillage. In [20], a power management system was designed for hydrogen-storage-based DC microgrid, which is suitable to keep power balance under the transient operation condition. However, the comprehensive renewable-energy-powered hydrogen generation and storage model considering the complementarity of different hydrogen products has not been studied yet.

In another context, providing ancillary service to the electricity market is recognized as a win-win situation to both the grid and consumers [4], which can be mainly classified into three categories, i.e., demand response (DR) [2]-[4], frequency/voltage support [20], [21], and operation reserve provision [1]. The joint devices in the hydrogen-based microgrid, like electrolyzer and fuel cell, can achieve bi-directional interaction with the grid, which can provide ancillary service to the grid. Several studies have investigated the application of ancillary service provision by hydrogen facilities. An optimal scheduling model incorporated DR signals for on-site gaseous hydrogen fueling stations (HFSs) was proposed in [2], whose rate of return was promoted. The optimal sizing and scheduling algorithm for LOHC-based hydrogen generation and storage plants were proposed in [4], which adaptively adjusted the state of charge (SOC) of tanks for ancillary service provision. In [1], a supervisory-based scheduling model considering operation reserve provision was developed to enhance the energy utilization efficiency during the off-peak hydrogen load period. However, the effectiveness of ancillary service provision under multi-state hydrogen generation and storage has not been investigated yet.

It is worth noting that there are multi-energy carriers within a hydrogen-based microgrid, whose coupling relation should be investigated for operation performance improvement. In the existing literature, the concept of energy hub is commonly deployed to model the multiple energy carrier systems [22]. Given the uncertainty introduced by renewable energy and loads, stochastic optimization and robust optimization are frequently utilized. In [23], a multi-input multi-output energy hub system was formulated and the scenario-based optimal scheduling algorithm was deployed for the biogas-solar-wind system to improve the energy efficiency. In [24], the interdependencies among power, gas, and water system were investigated in a water-energy nexus system with multiple energy hub systems, in which the uncertainty of wind energy was considered. Given the challenge introduced by the intermittency of renewable energy for the optimal operation of the energy hub system, a distributed robust optimization method was proposed in [25], which took into account the multimodal forecast errors of photovoltaic power. In [26], a probabilistic scheduling model considering multiple uncertainties was formulated for an integrated energy hub to determine the dispatch factors for operation efficiency enhancement. However, the optimization of coupling interactions of multi-type multi-state energy carriers in an energy hub considering uncertainty has not been investigated yet.

Based on the aforementioned discussions, to fill the gap of multi-state hydrogen generation and storage considering complementarity of multiple products, this paper proposes a novel multi-product optimal scheduling (MPOS) algorithm to enhance the economic feasibility for gaseous-liquid hydrogen generation and storage plants powered by renewable energies, which can provide concurrent service to both transportation sector and ancillary market. With the development of other hydrogen storage techniques, more hydrogen products with new characteristics can be easily incorporated into the formulated framework. The main objectives and contributions are listed as follows.

1) A novel power to multi-state hydrogen (P2MH) model is formulated to analyze the branched hydrogen flow constraints and energy consumption relation during the generation, processing, and storage process of hydrogen.

2) The multi-state energy coupling matrix is formulated to model the coupling and interaction of energy hub internal modules, including renewable energy system (RES) units, P2MH module, and consumers, which is the integration of energy hub internal devices and the foundation for the optimal scheduling algorithm. The dispatch factors of the matrix can be optimized with the proposed MPOS algorithm to enhance the energy efficiency and operation economy of the system.

3) A new MPOS algorithm considering the complementarity of different hydrogen products and DR service provision is proposed to enhance the economic feasibility of the facility. Besides, the scenario-based method is deployed to consider the uncertainty introduced by renewable energies, wholesale electricity price, and hydrogen loads.

The remainder of the paper is organized as follows. Section II presents the proposed energy hub model for gaseous-liquid hydrogen generation and storage plants. Section III presents the proposed MPOS algorithm. In Section IV, case studies are presented to demonstrate the operation flexibility and profitability of the proposed MPOS algorithm. The conclusions are summarized in Section V.

II. Proposed Energy Hub Model For Gaseous-liquid Hydrogen Generation and Storage Plants

A. Framework of Proposed Energy Hub for Gaseous-liquid Hydrogen Generation and Storage Plants

The gaseous-liquid hydrogen generation and storage plant can be regarded as an energy hub to analyze and schedule the conversion of energy carriers with different states, which is composed of three parts including RES units, P2MH module, and consumers, as depicted in Fig. 1. The facility is powered by a hybrid solar-wind RES and the insufficient en-

ergy can be purchased from the grid. The generation, processing, storage, and distribution of multi-state hydrogen can be modeled as P2MH module. In the P2MH module, the hydrogen is generated by electrolyzer in form of water electrolysis. The generated hydrogen is branched into two substreams and separately flows into the compressor and the refrigerator to be processed into the high-pressure gas and cryogenic liquid with desirable quality and quantity. When the processed hydrogen generation rate is higher than the demand, the surplus hydrogen is stored in storage tanks. Furthermore, the operation of the electrolyzer is incented to be curtailed by DR signals during on-peak hours to support the grid. The transformed electricity and the produced hydrogen commodities are delivered to the output ports of the energy hub for consumers. The generated gaseous and liquid hydrogen is transported to the retailers with tube trailers.

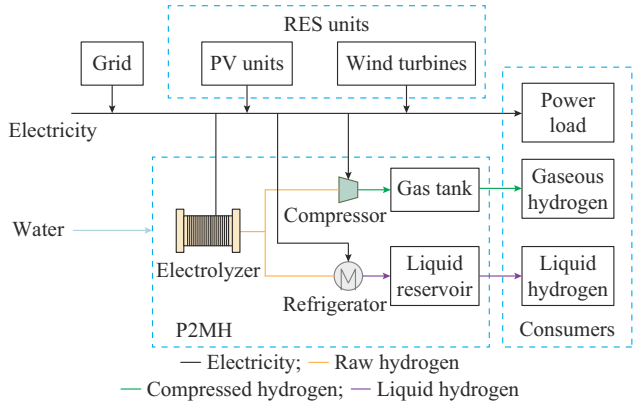

Fig. 1. Configuration of energy hub for gaseous-liquid hydrogen generation and storage plant.

B. Proposed P2MH Model

The mathematical model of P2MH process is used to analyze the hydrogen flow rate constraints and the energy conversion relation among electrolysis, compression, liquefaction, and storage processes, which can be incorporated into the proposed MPOS algorithm to minimize the operation costs, as depicted in Fig. 2.

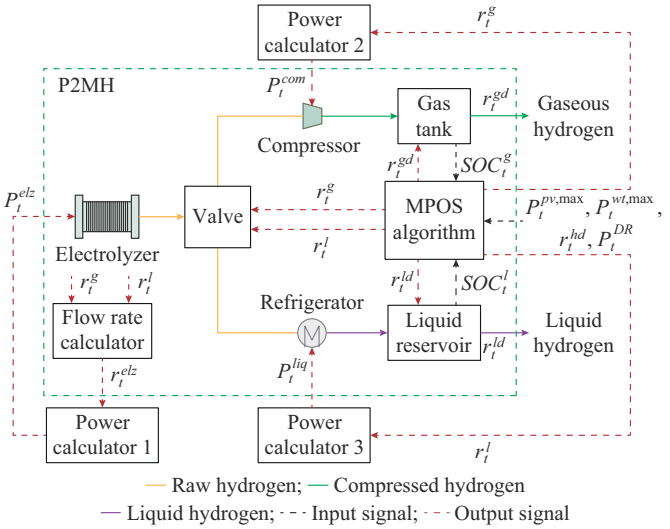

Fig. 2. Schematic diagram of P2MH model.

The target of the P2MH model is to derive the relationship between working power and hydrogen generation rate of electrolyzer, compressor, and refrigerator. Supposing the required gaseous and liquid hydrogen generation rates are r_t^g and r_t^l, respectively, which are acquired with the proposed MPOS algorithm, the required working power P_t^{elz}, P_t^{com}, and P_t^{liq} can be deduced based on the electrochemical and thermodynamic characteristics of the corresponding devices.

1) Electrolysis Process

The hydrogen is generated by the electrolyzer through water electrolysis. The proton exchange membrane electrolyzer (PEME) is selected for its faster adaptation capability and quicker ramp rate integrated with RESs [27]. The required hydrogen generation rate is determined by the hydrogen feeding rate required by compressor and refrigerator.

$$r_t^{elz} = r_t^g + f_{elz}(r_t^l) \tag{1}$$

To guarantee the hydrogen supply for the compressor and refrigerator, according to [2], the working power of the electrolyzer can be calculated (by power calculator 1 in Fig. 2) as:

$$P_t^{elz} = \frac{1}{\eta^{elz}} \Pi^{P2H} r_t^{elz} \tag{2}$$

2) Compression Process

The pressure of highly compressed hydrogen should be 700 bar for hydrogen-powered vehicles (HVs) [9]. The gas compression process can be usefully approximated by a polytropic process. The compressor performed work can be calculated (by power calculator 2 in Fig. 2) as:

$$P_t^{com} = \frac{1}{\eta^{com}} \frac{k_c R T^{P2H}}{k_c - 1} \left[\left(\frac{p_t^{stg}}{p_t^{elz}} \right)^{\frac{k_c - 1}{k_c}} - 1 \right] r_t^g = \frac{1}{\eta^{com}} \Pi^{com} r_t^g \tag{3}$$

3) Liquefaction Process

To investigate the required working power of the refrigerator as well as the deviation between the hydrogen feeding rate $f_{elz}(r_t^l)$ and the liquid hydrogen generation rate r^l, the thermodynamic process of the Claude cycle refrigerator [15] is analyzed, as shown in Fig. 3. Blue lines of different depths present the cooled hydrogen in different temperatures.

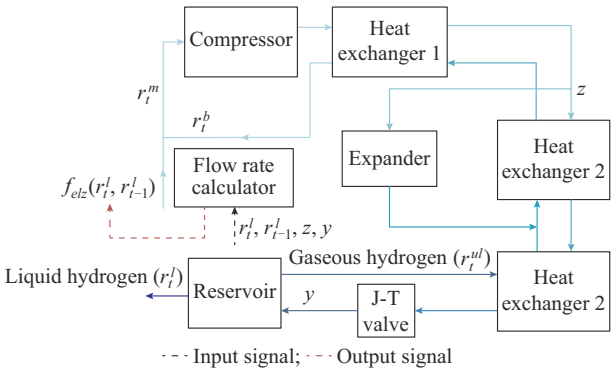

Fig. 3. Thermodynamic process of Claude cycle refrigerator.

The feeding gas supplied by electrolyzer and the uncondensed gas flowing back are mixed to form the mainstream gas flow r_t^m. The mixed gas flows through the compressor,

heat exchangers, and Joule Thomson (J-T) valve to be cooled. The expander is allocated to increase the cooling effect and decrease the inlet temperature of J-T valve. Based on the analysis above, the relationship among $f_{elz}(r_t^l)$, r_t^b, and r_t^m can be depicted as (4). Equation (5) illustrates the relation between the liquefied stream and the mainstream. The relation between the liquefied stream and the stream flowing back is described as (6).

$$r_t^m = f_{elz}(r_t^l) + r_t^b \tag{4}$$

$$r_t^l = r_t^m (1-z)y \tag{5}$$

$$r_t^b = \frac{(1-y)r_t^l}{y} \tag{6}$$

Substituting (5) and (6) into (4), the relation between $f_{elz}(r_t^l)$ and r_t^l can be deduced as:

$$f_{elz}(r_t^l) = r_t^l \tag{7}$$

It can be found that the required hydrogen feeding rate is equal to the liquid hydrogen generation rate without considering the variation of the required liquid hydrogen generation rate. In fact, the liquid hydrogen generation rate is changed with the variation of demands, and the required hydrogen feeding rate is not equal to the liquid hydrogen generation rate due to the uncondensed portion of hydrogen. At this time, the hydrogen feeding rate should compensate the liquefied part and the variation of the uncondensed portion. The detailed derivation process can be deduced as:

$$\begin{cases} r_t^m = f_{elz}(r_t^l) + r_{t-1}^b \\ r_t^l = r_t^m (1-z)y \\ r_{t-1}^b = \dfrac{(1-y)r_{t-1}^l}{y} \end{cases} \tag{8}$$

Based on (8), when the required liquid hydrogen generation rate changes, the required hydrogen feeding rate can be obtained by (9) (by flow rate calculator), as shown in Fig. 3.

$$f_{elz}(r_t^l, r_{t-1}^l) = \frac{1}{y(1-z)} r_t^l - \frac{1-y}{y} r_{t-1}^l \tag{9}$$

The relationship between working power and the required liquid hydrogen generation rate can be calculated (by power calculator 3 in Fig. 2) as:

$$P_t^{liq} = \frac{1}{\eta^{liq}} \Pi^{ref} r_t^l \tag{10}$$

4) Storage Process

When the generated hydrogen quantity is higher than the demand, the surplus hydrogen is stored in the tank. Otherwise, the insufficient hydrogen is supplemented by the hydrogen accumulated in the tank. The SOC of the hydrogen storage system can be presented as:

$$SOC_k^g = \frac{1}{Q^{g,\max}} \left[Q^{g,\text{int}} + \Delta T \sum_{t=1}^{k} (r_t^g - r_t^{gd}) \right] \tag{11}$$

$$SOC_k^l = \frac{1}{Q^{l,\max}} \left[Q^{l,\text{int}} + \Delta T \sum_{t=1}^{k} (r_t^l - r_t^{ld}) \right] \tag{12}$$

It is worth noting that the evaporation loss in the liquid hydrogen reservoir is taken into account in this paper since it is not possible to prevent all heat from flowing into the tank [3].

$$Q_{d+1}^l = (1-\gamma^{l,d}) Q_d^l \tag{13}$$

C. Multi-energy Coupling Matrix

The proposed energy hub model is a multi-input multi-output system, which is composed of several modules including renewable energies, P2MH module, and consumers. In order to achieve the optimal operation of the system, the couplings and interactions among different equipment should be explicitly analyzed. Based on the established system framework in Section II-A and the formulated P2MH model in Section II-B, a multi-energy coupling matrix can be derived to integrate all the modules in the system, which can exhibit the mapping of power from the input to the output, as shown in (14).

$$\underbrace{\begin{bmatrix} \eta^{pv}(1-v^g-v^l) & \eta^{wt}(1-v^g-v^l) & 1-v^g-v^l & 0 & 0 \\ \eta^{pv}v^g/(\Pi^{P2H}/\eta^{elz}+\Pi^{com}/\eta^{com}) & \eta^{wt}v^g/(\Pi^{P2H}/\eta^{elz}+\Pi^{com}/\eta^{com}) & v^g/(\Pi^{P2H}/\eta^{elz}+\Pi^{com}/\eta^{com}) & 1 & 0 \\ \eta^{pv}v^l/(\Pi^{P2H}f_{elz}(1)/\eta^{elz}+\Pi^{ref}/\eta^{ref}) & \eta^{wt}v^l/(\Pi^{P2H}f_{elz}(1)/\eta^{elz}+\Pi^{ref}/\eta^{ref}) & v^l/(\Pi^{P2H}f_{elz}(1)/\eta^{elz}+\Pi^{ref}/\eta^{ref}) & 0 & 1 \end{bmatrix}}_{C} \underbrace{\begin{bmatrix} P^{pv} \\ P^{wt} \\ P^g \\ r^{gs} \\ r^{ls} \end{bmatrix}}_{I} = \underbrace{\begin{bmatrix} L^e \\ r^{gd} \\ r^{ld} \end{bmatrix}}_{O} \tag{14}$$

As depicted in Fig. 1, the energy hub consumes the energy generated by renewable energy and purchases the insufficient energy from the grid, then delivers the transformed electric energy and the produced hydrogen commodities to consumers. The surplus energy can be stored in the state of gaseous or liquid hydrogen. We assign the input vector $\boldsymbol{I}$ consisting of the input power variables (P^{pv}, P^{wt}, P^g) and the input hydrogen variables (r^{gs}, r^{ls}). The output vector $\boldsymbol{O}$ is assumed to include L^e, r^{gd}, and r^{ld} ($r^{gd}+r^{ld}=r^{hd}$). The conversion from input vector to output vector can be modeled with multi-energy coupling matrix $\boldsymbol{C}$. In the matrix, the output power of converters is regarded as the product of their efficiencies and inputs.

The multi-energy coupling matrix is not only the integration of the energy hub internal energy flow but also the foundation for the optimal scheduling algorithm. The dispatch factors of the matrix can be optimized with the proposed MPOS algorithm illustrated in the next section to enhance the energy conversion efficiency and operation economy of the whole system.

III. Proposed MPOS Algorithm for Gaseous-liquid Hydrogen Generation and Storage Plants

Based on the couplings and interactions among system internal devices modeled by the multi-energy coupling matrix in the above section, the MPOS algorithm is formulated to

optimize the dispatch factors in the matrix to enhance the economic feasibility of the facility, as shown in Fig. 4. Specifically, information profiles including renewable energy curves, fuel demand of the transportation sector, electricity price, and DR signals are incorporated into the module of proposed MPOS algorithm. To take into account the characteristics of multi-state hydrogen, the hydrogen-related cost profiles are also input into the algorithm module. Besides, the scenario-based method is deployed to take into account the uncertainty introduced by renewable energy, wholesale market, and hydrogen loads. In this regard, Monte Carlo simulations are implemented to obtain a set of scenarios in which each scenario expresses a possible status of stochastic variables. Then a scenario reduction technique is further utilized to reduce the computational cost.

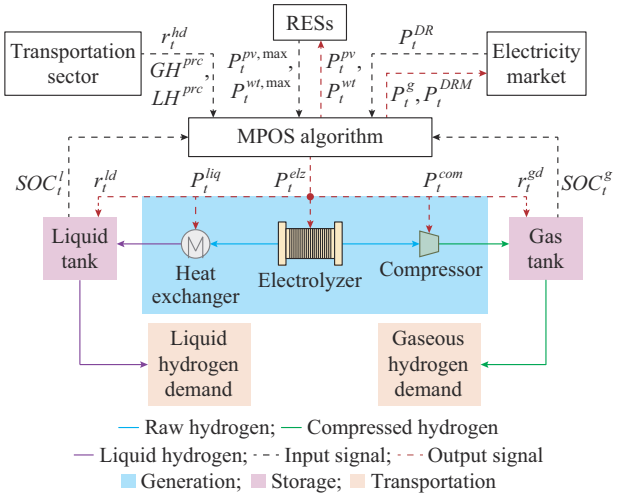

Fig. 4. Schematic diagram of proposed MPOS algorithm.

Based on the generated scenarios, the scheduling signals are generated with the proposed MPOS algorithm to schedule the generation, compression, liquefaction, storage, and transportation of hydrogen. Based on the above process, fuel supply to the transportation sector and DR to the grid are executed simultaneously.

A. Energy Scheduling Objective

Based on the proposed energy hub model, the objective of the proposed MPOS algorithm can be set to maximize the profit of the facility, as shown in (15). The control variables can be assigned as P^{pv}, P^{wt}, r^{gd}, r^{ld}, r^{g}, r^{l}, P^{DRM}, and P^{g}.

$$\max\left\{\sum_{s=1}^{NS}\rho_s\sum_{t=1}^{NT}(R_{s,t}^{TE}-C_{s,t}^{EP}-OPEX_{s,t}-C_{s,t}^{TP})\right\} \tag{15}$$

The characteristics of the proposed MPOS algorithm are summarized as follows: ① the complementarity of different hydrogen products is considered; ② ancillary service is provided to the grid for additional revenue; and ③ the uncertainty introduced by stochastic variables is considered. It is worth noting that on the one hand, not only the selling prices but also the generation, storage, and transportation of multiple state hydrogen are different. On the other hand, the electricity price is diverse in different time periods. Consequently, the generated quantity and time of different hydrogen products can be optimized to enhance the economic feasibility of the facility. Supposing the total hydrogen demand is a certain amount, the selling quantity of gaseous and liquid hydrogen can be optimized to maximize the operation revenue, and the generation rate in different time slots of different hydrogen products can be determined to minimize the operation costs.

Specifically, the objective function (15) consists of four terms. The first term $R_{s,t}^{TE}$ in (15) describes the operation revenue, which is composed of the hydrogen selling revenue $R_{s,t}^{H}$ and the ancillary service provision revenue $R_{s,t}^{DR}$, as shown in (16). $R_{s,t}^{H}$ is equal to the product of hydrogen selling price and commodity quantity, as shown in (17); while $R_{s,t}^{DR}$ is equal to the product of the incentive price and the electric energy served for DR, as shown in (18). The DR signal is assumed as P^{DR} and the slack variable P^{DRM} is introduced to increase the flexibility of service provision.

$$R_{s,t}^{TE}=R_{s,t}^{H}+R_{s,t}^{DR} \tag{16}$$

$$R_{s,t}^{H}=GH^{prc}\cdot r_{s,t}^{gd}+LH^{prc}\cdot r_{s,t}^{ld} \tag{17}$$

$$R_{s,t}^{DR}=DR^{prc}\cdot(P_{s,t}^{DR}-P_{s,t}^{DRM}) \tag{18}$$

The second term $C_{s,t}^{EP}$ in (15) describes the electric energy consumption costs, which is composed of three parts, as shown in (19). The first two terms in (19) are the operation costs of photovoltaic units and wind turbines [28], [29]. Given the decline in investment costs for renewable energy, operation and maintenance (O&M) costs become increasingly important. To take into account this portion of costs, the self-used renewable energy is regarded as the operation costs considering that if this part of energy is sold to the grid, an extra income can be achieved. The third term in (19) describes the costs of energy purchased from the grid.

$$C_{s,t}^{EP}=C^{pv}P_{s,t}^{pv}+C^{wt}P_{s,t}^{wt}+C_{s,t}^{e}P_{s,t}^{g} \tag{19}$$

The equipment utilization will result in wear and tear. The third term $OPEX_{s,t}$ in (15) describes the operation expenditure (OPEX) due to hydrogen generation, processing, and storage, which can be expressed as:

$$\begin{aligned}OPEX_{s,t}=&OC^{elz}\cdot P_{s,t}^{elz}+OC^{com}\cdot P_{s,t}^{com}+\\&OC^{ref}\cdot P_{s,t}^{liq}+OC^{g}\cdot Q_{s,t}^{g}+OC^{l}\cdot Q_{s,t}^{l}\end{aligned} \tag{20}$$

The generated hydrogen should be transported to the retailers with tube trailers, e.g., HFS. The fourth term $C_{s,t}^{TP}$ in (15) describes the total transport costs of hydrogen commodities, which can be expressed as:

$$C_{s,t}^{TP}=TC^{g}\cdot r_{s,t}^{gd}+TC^{l}\cdot r_{s,t}^{ld} \tag{21}$$

B. System Constraints

1) Power Balance Constraints

The power supplied by photovoltaic units, wind turbines, and the grid should guarantee the generation, processing, and storage of hydrogen in each time slot.

$$\frac{\Pi^{P2H}(r_{s,t}^{g}+f_{elz}(r_{s,t}^{l}))}{\eta^{elz}}+\frac{\Pi^{com}r_{s,t}^{g}}{\eta^{com}}+\frac{\Pi^{ref}r_{s,t}^{l}}{\eta^{ref}}=P_{s,t}^{pv}+P_{s,t}^{wt}+P_{s,t}^{g} \tag{22}$$

2) RES Capacity Constraints

The output power of photovoltaic units and wind turbines should be within their maximum capability.

$$0 \le P_{s,t}^{pv} \le P_{s,t}^{pv,\max} \tag{23}$$

$$0 \le P_{s,t}^{wt} \le P_{s,t}^{wt,\max} \tag{24}$$

3) Grid Power Constraints

The power purchased from the grid should not exceed the maximum interaction capacity and is nonnegative.

$$0 \le P_{s,t}^{g} \le P^{g,\max} \tag{25}$$

4) Hydrogen Supply Constraints

The gaseous and liquid hydrogen supplied to consumers should be nonnegative, whose summation should not be larger than the total hydrogen demand.

$$r_{s,t}^{gd} + r_{s,t}^{ld} \le r_{s,t}^{hd} \tag{26}$$

$$\begin{cases} r_{s,t}^{gd} \ge 0 \\ r_{s,t}^{ld} \ge 0 \end{cases} \tag{27}$$

5) Equipment Capacity Constraints

Hydrogen generation rate of electrolyzer, hydrogen processing rate of compressor, and refrigerator should be within their physical limitations, as shown in (28)-(30), respectively. It is worth noting that the operation of the electrolyzer is also impacted by the DR signals commanded by the grid, as shown in (28). The slack variable of DR power should not exceed the value of DR signals, as shown in (31). The gaseous and liquid hydrogen generation rate should be nonnegative, as shown in (32).

$$r^{elz,\min} \le r_{s,t}^{elz} \le r^{elz,\max} - \frac{\eta^{elz}(P_{s,t}^{DR} - P_{s,t}^{DRM})}{\Pi^{P2H}} \tag{28}$$

$$r^{com,\min} \le r_{s,t}^{g} \le r^{com,\max} \tag{29}$$

$$r^{ref,\min} \le r_{s,t}^{l} \le r^{ref,\max} \tag{30}$$

$$0 \le P_{s,t}^{DRM} \le P_{s,t}^{DR} \tag{31}$$

$$\begin{cases} r_{s,t}^{g} \ge 0 \\ r_{s,t}^{l} \ge 0 \end{cases} \tag{32}$$

6) Hydrogen Storage Constraints

The SOC of both gas tank and liquid reservoir should be within their physical limitations for security in every time slot.

$$SOC^{g,\min} \le SOC_{s,t}^{g} \le SOC^{g,\max} \tag{33}$$

$$SOC^{l,\min} \le SOC_{s,t}^{l} \le SOC^{l,\max} \tag{34}$$

IV. Case Studies

A. System Data and Configuration

In this paper, the proposed energy hub model depicted in Fig. 1 is utilized to validate the performance of the proposed MPOS algorithm for every hour over a week. The facility is comprised of an electrolyzer, a compressor, a refrigerator, gas tanks, and liquid reservoirs. A hybrid RES composed of photovoltaic units and wind turbines is allocated for the power supply. Wind and solar data are set with history data given in [4]. The hydrogen demand of the facility is presented by aggregation of the transportation sector, e.g., HFSs, whose profiles are set with history data given in [4]. The wholesale electricity price is forecasted with historical price data taken from [2]. The modeling and simulation parameters are summarized and listed in Table I [1]-[3].

To take into account the uncertainty factors, the wind speed, solar radiation, electricity price, and hydrogen demand are assumed to be approximately normal distribution, whose averages are equal to forecasting values and the standard deviations are 10%, 10%, 5%, 10%, respectively. The problem is formulated as a scenario-based stochastic optimization formulation, which can be implemented with the YALMIP toolbox in MATLAB. The CPLEX solver on an 8 GHz Intel Core i7 CPU and 8 GB RAM personal computer is utilized to solve the problem.

TABLE I
Modeling and Simulation Parameters

Unit	Parameter
Electrolyzer	$\Pi^{P2H}=32.04$ kWh/kg, $\eta^{elz}=60\%$, $r^{elz,\max}=250$ kg/h, $r^{elz,\min}=0$ kg/h, $C^{elz}=600$ \$/kW, $OC^{elz}=3\%\times C^{elz}/8760$ \$/kWh
Compressor	$\Pi^{com}=3.74$ kWh/kg, $\eta^{com}=63\%$, $r^{com,\max}=250$ kg/h, $r^{com,\min}=0$ kg/h, $C^{com}=4.6$ k\$/kW, $OC^{com}=4\%\times C^{com}/8760$ \$/kWh
Refrigerator	$\Pi^{ref}=13.24$ kWh/kg, $\eta^{ref}=60\%$, $z=0.2$, $y=0.6$, $r^{ref,\max}=250$ kg/h, $r^{ref,\min}=0$ kg/h, $C^{ref}=2.5$ M\$/(t/d), $OC^{ref}=8\%\times C^{ref}/8760$ \$/kg
Gas tank	$Q^{g,\max}=2500$ kg, $Q^{g,\min}=250$ kg, $C^{g}=595$ \$/kg, $OC^{g}=2\%\times C^{g}/8760$ \$/kg
Liquid reservoir	$Q^{l,\max}=2500$ kg, $Q^{l,\min}=250$ kg, $\gamma^{l,d}=0.03\%$ d^{-1}, $C^{l}=30$ \$/kg, $OC^{l}=2\%\times C^{l}/8760$ \$/kg
Transport	$TC^{g}=0.68$ \$/kg, $TC^{l}=0.15$ \$/kg [30]
Hydrogen price	$GH^{prc}=10$ \$/kg, $LH^{prc}=12$ \$/kg
DR price	$DR^{prc}=0.03$ \$/kWh [2]
Renewable generation cost	$C^{pv}=0.05$ \$/kWh, $C^{wt}=0.05$ \$/kWh [28], [29]

B. Analysis of Scheduling Results

The proposed MPOS algorithm illustrated in Section III is utilized to determine the optimal working points of devices in the plant for profit maximization. The electricity price curve shown in Fig. 5(a) is higher during peak hours and lower during off-peak hours. The fuel delivery from the facility to the consumer site is assumed to take place at the end of the day [4], as shown in Fig. 5(b).

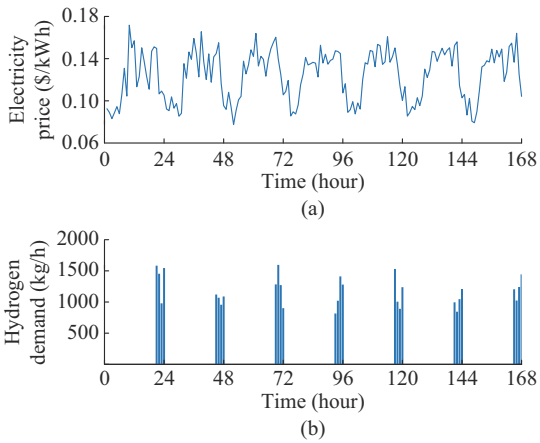

Fig. 5. Electricity price and hydrogen demand over a week. (a) Electricity price. (b) hydrogen demand.

The optimal scheduling results of the gaseous-liquid hydrogen generation and storage plant with the proposed MPOS algorithm over a week are depicted in Fig. 6. Figure 6(a) describes the hydrogen generation rate of electrolyzer. It can be observed that it is composed of two parts. One is supplied to the compressor and another is fed to the refrigerator. Figure 6(b) presents the generation rate of the high-pressure gaseous hydrogen, which is also the hydrogen feeding rate required by the compressor. Figure 6(c) depicts two curves, which are the liquid hydrogen generation rate and the hydrogen feeding rate required by refrigerator, respectively. It can be observed that these two curves are different, which demonstrates that the proposed P2MH model can effectively distinguish the deviation between these two issues due to the impact of the uncondensed hydrogen gas in the refrigerator. Furthermore, it is worth noting that the high-power operations of not only electrolyzer but also compressor and refrigerator all occur during lower-electricity-price periods to reduce hydrogen generation costs, which matches the expectation.

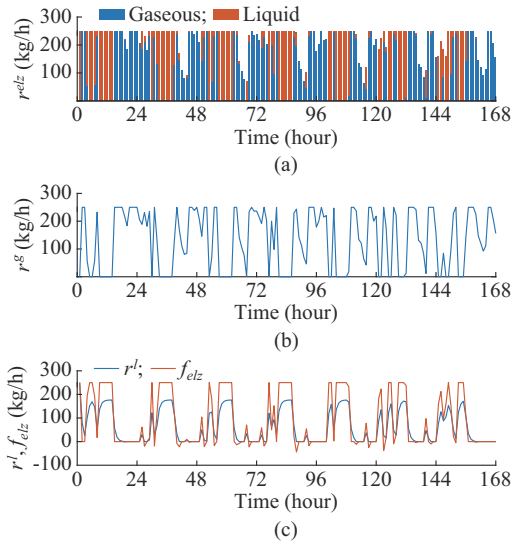

Fig. 6. Optimal scheduling results of gaseous-liquid hydrogen generation and storage plant with proposed MPOS algorithm over a week. (a) Electrolyzer. (b) Compressor. (c) Refrigerator.

Figure 7 shows the scheduling results of electrolyzer with and without consideration of DR signals over a week.

Supposing DR signals occur during peak-electric-load periods, it can be observed that the electrolyzer can be incentivized to be shifted during peak-electric-load period when considering the DR signals, which can effectively support the grid and earn additional revenue.

The SOC curves of the hydrogen storage devices over a week are depicted in Fig. 8. It can be observed that the SOCs of gas tank and liquid reservoir both decrease when the hydrogen demand exceeds the generation and vice versa. It is worth noting that the accumulated gaseous hydrogen in the gas tank in every time slot is less than the liquid hydrogen. This is because the storage cost of liquid hydrogen are less than that of highly compressed gaseous hydrogen, which is in favor of operation cost reduction.

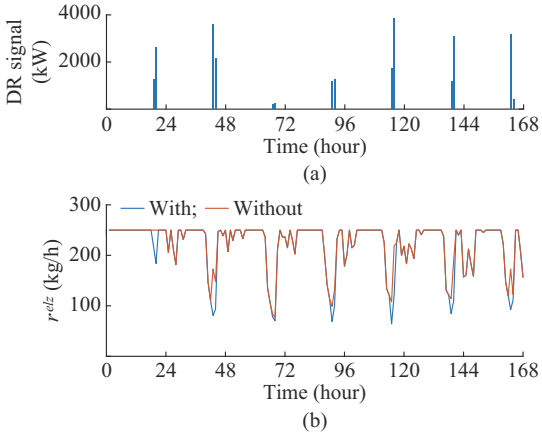

Fig. 7. Scheduling results of electrolyzer with and without consideration of DR signals over a week. (a) DR signals. (b) Hydrogen generation rate of electrolyzer with and without consideration of DR signals.

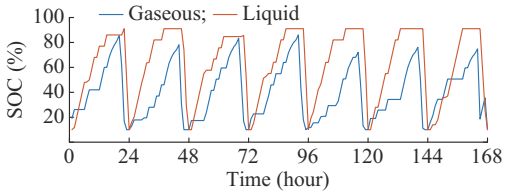

Fig. 8. SOC curves of hydrogen storage devices over a week.

C. Comparative Results and Analysis

For in-depth investigations on the effectiveness and superiority of the proposed methodology, five cases are adopted for comparative analysis and discussions. The optimization is performed over a week.

1) Case 1: gaseous-liquid hydrogen generation and storage plant with the consideration of DR signals.

2) Case 2: gaseous hydrogen generation and storage plant without the consideration of DR signals [31].

3) Case 3: gaseous hydrogen generation and storage plant with the consideration of DR signals [1].

4) Case 4: liquid hydrogen generation and storage plant without the consideration of DR signals [16].

5) Case 5: liquid hydrogen generation and storage plant with consideration of DR signals.

1) Economic Comparison

The RES generation costs, hydrogen generation, storage, transportation costs, power purchase costs, hydrogen selling revenue, and DR provision revenue are considered to analyze the economic feasibility of the proposed MPOS algorithm. The economic results are presented in Table II.

It can be observed that the total profit during one week in case 1 is the largest, which can earn $4084, $3415, $326981, and $26350 more than cases 2, 3, 4, and 5, respectively. Within one year, the stack income of the proposed MPOS algorithm can reach $212941, $178043, $1406880, and $1373963 more than cases 2, 3, 4, and 5, respectively. This validates the effectiveness of the proposed MPOS algorithm. For single-product generation, the generation cost for high-pressure gaseous hydrogen (cases 2 and 3) are lower than that of cryogenic liquid hydrogen (cases 4 and 5), but the storage and transportation costs of gaseous hydrogen are

higher. Besides, the selling revenue of gaseous hydrogen (cases 2 and 3) is less than that of liquid hydrogen (cases 4 and 5). This is consistent with the characteristics of hydrogen with different states. For the proposed MPOS algorithm, the operation costs are larger than those in gaseous-hydrogen-based operation mode (cases 2 and 3) and smaller than those in liquid-hydrogen-based operation mode (cases 4 and 5). The revenues are also larger than those in gaseous-hydrogen-based operation mode and smaller than those in liquid-hydrogen-based operation mode. But the total profit with the proposed MPOS algorithm is the largest (case 1). This demonstrates that the advantages of different products can be deployed comprehensively with the proposed MPOS algorithm. Furthermore, the profit of the cases with consideration of DR signals is higher than that without consideration of DR signals, which is constant with the expectation.

TABLE II
ECONOMIC RESULTS

Case	Cost ($)					Revenue ($)		Total profit ($)
	RES generation	Hydrogen generation	Hydrogen storage	Hydrogen transportation	Power purchase	Hydrogen selling	DR provision	
1	80210	97610	300	16190	17400	361380	630	247120
2	68730	70720	580	22940	1990	337390	0	243040
3	68730	70720	580	22940	1990	337390	670	243710
4	90040	177710	30	5060	87670	404880	0	220140
5	90040	177710	30	5060	87670	404880	630	220770

Figure 9 presents the SOC curves of hydrogen storage in different cases. It can be observed that, compared with other cases, the accumulated quantity of gaseous hydrogen is the smallest while the accumulated quantity of liquid hydrogen is the largest in most time slots in case 1. This is consistent with the characteristics of hydrogen products that the storage costs of gaseous hydrogen are lower than liquid hydrogen.

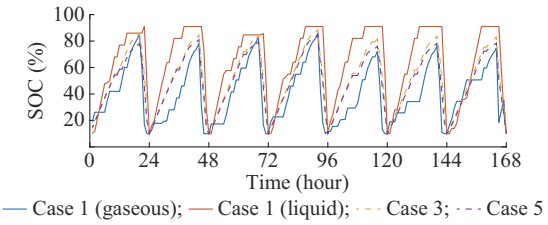

Fig. 9. SOC curves of hydrogen storage in different cases.

2) Renewable Energy Accommodation Comparison

To investigate the impact of proposed MPOS algorithm on renewable energy accommodation, the renewable energy consumption ratio W_{acc} is used as the index.

$$W_{acc}=\frac{\sum_{s=1}^{NS}\sum_{t=1}^{NT}(P_{s,t}^{wt}+P_{s,t}^{pv})}{\sum_{s=1}^{NS}\sum_{t=1}^{NT}(P_{s,t}^{wt,\max}+P_{s,t}^{pv,\max})}\times 100\% \tag{35}$$

The comparison of renewable energy accommodation results in different cases are depicted in Table III. It can be observed that the consumption ratio of RES in case 1 is larger than that in cases 2 and 3 while less than that in cases 4 and 5. Since the energy consumption of highly compressed gaseous hydrogen is lower than that of liquid hydrogen and the storage cost of gaseous hydrogen is higher than that of liquid hydrogen, the highly compressed gaseous hydrogen is unfavorable for renewable energy accommodation, which have the characteristics of high intermittence and fluctuation. And the situation is opposite for liquid hydrogen. Therefore, compared with cases 2 and 3, where gaseous hydrogen is produced individually, the proposed MPOS algorithm can promote renewable energy accommodation to some extent, as shown in Table III. But the energy consumption and transportation cost of liquid hydrogen is high, which is unfavorable for economic operation. Consequently, compared with cases 4 and 5, where liquid hydrogen is produced individually, the proposed MPOS algorithm can enhance the economic feasibility, as shown in Table II.

TABLE III
RENEWABLE ENERGY ACCOMMODATION RESULTS

Case	Consumed energy (MWh)	Total energy (MWh)	Consumed ratio (%)
1	1500.9	1782.7	84.19
2	1393.6	1782.7	78.18
3	1393.6	1782.7	78.18
4	1516.2	1782.7	85.05
5	1516.2	1782.7	85.05

D. Sensitive Analysis

In order to analyze the influence of RES capability, electrolyzer capacity, and DR signals on the operation performance of the facility, the proposed MPOS algorithm is performed under the change of the above parameters, whose values are respectively set to be 80%, 100%, and 120% of the initial values.

1) Influence of RES Capacity

The impact of RES capacity change on the facility profits are illustrated in Table IV. It can be observed that, due to the lower costs of energy generated by renewable energies compared with energy purchased from the grid, the profit increases with the increase of RES capacity in all cases. Specifically, when the RES capability increases from 80% to 120% of the initial value, the profit grows $15918, $2568, $2568, $43818, and $43824 in cases 1, 2, 3, 4, and 5, respectively.

TABLE IV
IMPACT OF RES CAPACITY CHANGE ON FACILITY PROFITS

Case	Profit ($)		
	80%	100%	120%
1	233440	243810	249360
2	233150	235680	235720
3	234100	236620	236670
4	193810	217870	237630
5	194750	218820	238570

It can be found that the profit increment with the proposed MPOS algorithm (case 1) is larger than that in gaseous-hydrogen-based operation mode (cases 2 and 3) and smaller than that in liquid-hydrogen-based operation mode (cases 4 and 5). Furthermore, the total revenue of case 1 remains the largest compared with other cases, which demonstrates the economic feasibility of the proposed MPOS algorithm.

2) Influence of Electrolyzer Capacity

The impact of electrolyzer capacity change on the facility profits is shown in Table V.

TABLE V
IMPACT OF ELECTROLYZER CAPACITY CHANGE ON FACILITY PROFITS

Case	Profit ($)		
	80%	100%	120%
1	215270	248340	256020
2	229300	244430	245200
3	229670	245250	246020
4	199490	216360	223550
5	200040	217190	224380

It can be observed that, with the increase of electrolyzer capacity, the profits in different cases all increase. This is because more generation can be gathered in lower-electricity-price hours with larger electrolyzer capacity for lower hydrogen generation costs, which is consistent with the expectation. However, the investment costs will increase and the time utilization efficiency of the electrolyzer will decrease, which is unfavorable for economic operation. But it is out of the scope of this paper. Furthermore, it is worth noting that the total profit in case 1 remains the largest with different electrolyzer capacities, which is in favor of the validation of the effectiveness of the proposed MPOS algorithm.

3) Influence of DR Signals

Table VI presents the impact of DR signal change on the facility profits. It can be observed that the week stacked profits increase with the required power indicated by DR signals.

This indicates that the more DR ancillary service is provided, the more DR revenue can be acquired. The participation of DR ancillary service can further enhance the economic feasibility of the facility. It is worth noting that the profit in case 1 keeps the largest regardless of the change of DR signals, which demonstrates the effectiveness of the proposed MPOS algorithm.

TABLE VI
IMPACT OF DR SIGNAL CHANGE ON FACILITY PROFITS

Case	Profit ($)		
	80%	100%	120%
1	246540	246710	246880
2	236810	236810	236810
3	237490	237660	237830
4	223030	223030	223030
5	223710	223880	224050

V. CONCLUSION

The cost-efficient hydrogen supply is the foundation for the application of hydrogen-based transportation. In this paper, the MPOS algorithm considering complementarity of different products is proposed to enhance economic feasibility for the gaseous-liquid hydrogen generation and storage plant powered by renewable energies, which can simultaneously achieve fuel supply to the transportation sector and ancillary service to the grid. The numerical studies demonstrate the stacked benefits of the proposed MPOS algorithm. The scheduling results validate that the proposed MPOS algorithm can realize the economic operation of hydrogen generation, processing, and storage through working during lower-electricity-price periods and the optimal distribution of gaseous and liquid hydrogen products. The comparative results show that the return rate of the facility increases with the complementarity of different hydrogen products. Besides, the MPOS algorithm with DR signals can achieve further profit enhancement. Furthermore, more hydrogen products with new characteristics can be easily incorporated into the formulated framework, which can be studied in future work.

REFERENCES

[1] H. Khani, N. A. El-Taweel, and H. E. Z. Farag, "Supervisory scheduling of storage-based hydrogen fueling stations for transportation sector and distributed operating reserve in electricity markets," *IEEE Transactions on Industrial Informatics*, vol. 16, no. 3, pp. 1529-1538, Mar. 2020.

[2] N. A. El-Taweel, H. Khani, and H. E. Z. Farag, "Hydrogen storage optimal scheduling for fuel supply and capacity-based demand response program under dynamic hydrogen pricing," *IEEE Transactions on Smart Grid*, vol. 10, no. 4, pp. 4531-4542, Jul. 2019.

[3] M. Reuß, T. Grube, M. Robinius *et al*., "Seasonal storage and alternative carriers: a flexible hydrogen supply chain model," *Applied Energy*, vol. 200, pp. 290-302, May 2017.

[4] N. A. El-Taweel, H. Khani, and H. E. Z. Farag, "Optimal sizing and scheduling of LOHC-based generation and storage plants for concurrent services to transportation sector and ancillary services market," *IEEE Transactions on Sustainable Energy*, vol. 11, no. 3, pp. 1381-1393, Jul. 2020.

[5] A. Fikrt, R. Brehmer, V.-O. Milella *et al*., "Dynamic power supply by hydrogen bound to a liquid organic hydrogen carrier," *Applied Energy*, vol. 194, pp. 1-8, May 2017.

[6] J. Li, J. Lin, H. Zhang *et al*., "Optimal investment of electrolyzers and seasonal storages in hydrogen supply chains incorporated with renewable electric networks," *IEEE Transactions on Sustainable Energy*, vol. 11, no. 3, pp. 1773-1784, Oct. 2020.

[7] G. Pan, W. Gu, Y. Lu *et al*., "Optimal planning for electricity-hydrogen integrated energy system considering power to hydrogen and heat and seasonal storage," *IEEE Transactions on Sustainable Energy*, vol. 11, no. 4, pp. 2662-2676, Jan. 2020.

[8] M. E. Demir and I. Dincer, "Cost assessment and evaluation of various hydrogen delivery scenarios," *International Journal of Hydrogen*

Energy, vol. 43, no. 22, pp. 10420-10430, May 2018.
[9] A. Bauer, T. Mayer, M. Semmel *et al*., "Energetic evaluation of hydrogen refueling stations with liquid or gaseous stored hydrogen," *International Journal of Hydrogen Energy*, vol. 44, no. 13, pp. 6795-6812, Mar. 2019.
[10] J. O. Abe, A. P. I. Popoola, E. Ajenifuja *et al*., "Hydrogen energy, economy and storage: review and recommendation," *International Journal of Hydrogen Energy*, vol. 44, no. 29, pp. 15072-15086, Jun. 2019.
[11] X. Li, J. D. Allen, J. A. Stager *et al*., "Paths to low-cost hydrogen energy at a scale for transportation applications in the USA and China via liquid-hydrogen distribution networks," *Clean Energy*, vol. 4, no. 1, pp. 26-47, Mar. 2020.
[12] Y. Zhao, M. Gong, Y. Zhou *et al*., "Thermodynamics analysis of hydrogen storage based on compressed gaseous hydrogen, liquid hydrogen and cryo-compressed hydrogen," *International Journal of Hydrogen Energy*, vol. 44, no. 31, pp. 16833-16840, Jun. 2019.
[13] M. Aziz, T. Oda, and T. Kashiwagi, "Comparison of liquid hydrogen, methylcyclohexane and ammonia on energy efficiency and economy," *Energy Procedia*, vol. 158, pp. 4086-4091, Feb. 2019.
[14] M. Aasadnia and M. Mehrpooya, "Large-scale liquid hydrogen production methods and approaches: a review," *Applied Energy*, vol. 212, pp. 57-83, Feb. 2018.
[15] C. Yilmaz, T. H. Cetin, B. Ozturkmen *et al*., "Thermodynamic performance analysis of gas liquefaction cycles for cryogenic applications," *Journal of Thermal Engineering*, vol. 5, no. 1, Jan. 2019, pp. 62-75.
[16] M. Nouri, M. Miansari, and B. Ghorbani, "Exergy and economic analyses of a novel hybrid structure for simultaneous production of liquid hydrogen and carbon dioxide using photovoltaic and electrolyzer systems," *Journal of Cleaner Production*, vol. 259, p. 120862, Jun. 2020.
[17] Y. Han, G. Zhang, Q. Li *et al*., "Hierarchical energy management for PV/hydrogen/battery island DC microgrid," *International Journal of Hydrogen Energy*, vol. 44, no. 11, pp. 5507-5516, Feb. 2019.
[18] M. Tostado-Véliz, P. Arévalo, and F. Jurado, "A comprehensive electrical-gas-hydrogen microgrid model for energy management applications," *Energy Conversion and Management*, vol. 228, p. 113726, Jan. 2021.
[19] E. Haghi, K. Raahemifar, and M. Fowler, "Investigating the effect of renewable energy incentives and hydrogen storage on advantages of stakeholders in a microgrid," *Energy Policy*, vol. 113, pp. 206-222, Feb. 2018.
[20] M. Alam, K. Kumar, S. Verma *et al*., "Renewable sources based DC microgrid using hydrogen energy storage: modelling and experimental analysis," *Sustainable Energy Technologies and Assessments*, vol. 42, p. 100840, Dec. 2020.
[21] D. Azuatalam, A. C. Chapman, and G. Verbič, "Probabilistic assessment of impact of flexible loads under network tariffs in low-voltage distribution networks," *Journal of Modern Power Systems and Clean Energy*, vol. 9, no. 4, pp. 951-962, Jul. 2021.
[22] N. Jia, C. Wang, W. Wei *et al*., "Decentralized robust energy management of multi-area integrated electricity-gas systems," *Journal of Modern Power Systems and Clean Energy*, vol. 9, no. 6, pp. 1478-1489, Nov. 2021.
[23] B. Zhou, D. Xu, C. Li *et al*., "Optimal scheduling of biogas-solar-wind renewable portfolio for multicarrier energy supplies," *IEEE Transactions on Power Systems*, vol. 33, no. 6, pp. 6229-6239, Nov. 2018.
[24] P. Zhao, C. Gu, Z. Cao *et al*., "Water-energy nexus management for power systems," *IEEE Transactions on Power Systems*, vol. 36, no. 3, pp. 2542-2554, May 2021.
[25] P. Zhao, C. Gu, D. Huo *et al*., "Two-stage distributionally robust optimization for energy hub systems," *IEEE Transactions on Industrial Informatics*, vol. 16, no. 5, pp. 3460-3469, May 2020.
[26] M. Alipour, K. Zare, and M. Abapour, "MINLP probabilistic scheduling model for demand response programs integrated energy hubs," *IEEE Transactions on Industrial Informatics*, vol. 14, no. 1, pp. 79-88, Jan. 2018.
[27] S. Clegg and P. Mancarella, "Integrated modeling and assessment of the operational impact of power-to-gas (P2G) on electrical and gas transmission networks," *IEEE Transactions on Sustainable Energy*, vol. 6, no. 4, pp. 1234-1244, May 2015.
[28] B. Steffen, M. Beuse, P. Tautorat *et al*., "Experience curves for operations and maintenance costs of renewable energy technologies," *Joule*, vol. 4, no. 2, pp. 359-375, Feb. 2020.
[29] OECD Statistics. (2020, Apr.). Renewable energy feed-in tariffs. [Online]. Available: https://stats.oecd.org/Index.aspx?DataSetCode=RE_FIT
[30] W. Amos. (1998, May). Costs of storing and transporting hydrogen. [Online]. Available: https://www.nrel.gov/docs/fy99osti/25106.pdf
[31] W. Xiao, Y. Cheng, W. Lee *et al*., "Hydrogen filling station design for fuel cell vehicles," *IEEE Transactions on Industry Applications*, vol. 47, no. 1, pp. 245-251, Feb. 2011.

Jiamei Zhang received the B.E. degree from the College of Electrical and Power Engineering, Taiyuan University of Technology, Taiyuan, China, in 2016. She is currently pursuing the Ph.D. degree at the College of Electrical and Information Engineering, Hunan University, Changsha, China. Her research interests include integrated energy system operation and optimization.

Kai Sun received the B.E., M.E., and Ph.D. degrees in electrical engineering from Tsinghua University, Beijing, China, in 2000, 2002, and 2006, respectively. He is currently a Tenured Associate Professor in electrical engineering at Tsinghua University. His research interests include power electronics for renewable generation systems, microgrids, and Energy Internet.

Canbing Li received the B.E. and Ph.D. degrees in electrical engineering from Tsinghua University, Beijing, China, in 2001 and 2006, respectively. He is currently working as a Professor at the School of Electronic Information and Electrical Engineering, Shanghai Jiao Tong University, Shanghai, China. His current research interests include power systems, smart grid, renewable energy, with an emphasis on large-scale power system dispatch, economic and secure operation of power systems, energy efficiency and energy conservation in smart grid, electric demand management of data center, and vehicle-to-grid technologies.

Hui Liu received the M.S. and Ph.D. degrees in electrical engineering from the College of Electrical Engineering, Guangxi University, Nanning, China, in 2004 and 2007, respectively. He is currently working as a Professor at the College of Electrical Engineering, Guangxi University. His research interests include power system control, electric vehicles, demand response, and power system optimization.

Wentao Huang received the Ph.D. degree in electrical engineering from Shanghai Jiao Tong University, Shanghai, China, in 2015. He is currently working as an Associate Professor at the Department of Power Electrical Engineering, Shanghai Jiao Tong University. His research interests include protection and control of active distribution systems, microgrids, smart grid, and renewable energy.

Bin Zhou received the B.Sc. degree in electrical engineering from Zhengzhou University, Zhengzhou, China, in 2006, the M.S. degree in electrical engineering from South China University of Technology, Guangzhou, China, in 2009, and the Ph.D. degree from The Hong Kong Polytechnic University, Hong Kong, China, in 2013. He is currently working as an Associate Professor at the College of Electrical and Information Engineering, Hunan University, Changsha, China. His research interests include smart grid operation and planning, renewable energy generation, and energy efficiency.

Xiaochao Hou received the B.S., M.S., and Ph.D. degrees in control science and engineering from the School of Automation, Central South University, Changsha, China, in 2014, 2017, and 2020, respectively. From 2018 to 2019, he was a joint Ph.D. student with the School of Electrical and Electronic Engineering, Nanyang Technological University, Singapore. He is currently a Postdoctoral Research Fellow with Tsinghua University, Beijing, China. His research interests include control and stability of distributed microgrid and series/parallel-type power grid.